



A spatial and temporal analysis of different periglacial materials by using geoelectrical, seismic and borehole temperature data at Murtèl–Corvatsch, Upper Engadin, Swiss Alps

S. Schneider, S. Daengeli, C. Hauck, and M. Hoelzle

Alpine Cryosphere and Geomorphology (ACAG), Department of Geosciences,
University of Fribourg, Switzerland

Correspondence to: S. Schneider (sina.schneider@unifr.ch)

Received: 4 March 2013 – Revised: 1 October 2013 – Accepted: 23 October 2013 – Published: 16 December 2013

Abstract. Different geophysical investigations, such as electrical resistivity tomography (ERT) and refraction seismic tomography (RST), allow for an improved characterization of subsurface conditions in mountain permafrost areas. The knowledge of the permafrost internal composition constitutes a major prerequisite for climate-related modelling studies, for detailed hazard or local infrastructure assessments. To detect the small-scale variations of permafrost characteristics and its varying sensitivity to climate influencing factors, two ERT and RST monitoring profiles were installed in 2009 at two different sites called Chastelets and Murtèl forefield located in the Murtèl–Corvatsch area, Upper Engadin, eastern Swiss Alps. The geophysical profiles extend over four existing boreholes and are characterized by strong small-scale variations of surface as well as subsurface structures such as bedrock, fine material or coarse debris. Here we present ERT measurements carried out in a bimonthly interval during the years of 2009 to 2012 and RST measurements which were performed once a year, normally in August, during the same period. Based on these data sets the so-called four-phase model, based on petrophysical relationships, was applied to determine the volumetric fractions of ice, water and air within the heterogeneous ground, resulting in a relatively precise description of the subsurface material around the existing boreholes.

The observations revealed a permafrost occurrence at the Chastelets rock glacier with an estimated ice-saturated layer of at least 10 m thickness and the detection of a thawed layer with increased water content in the lower frontal part of the rock glacier within an area of fine material. In the area of the Murtèl forefield the analysis revealed strongly weathered bedrock, which is in the upper part covered by a pronounced layer of coarse debris establishing a thermal regime which is able to sustain permafrost beneath. In addition, the high temporal ERT measurements revealed a seasonal formation of ice during wintertime within the coarse- as well as the fine-grained active layer zones. It can be concluded that the combination of existing borehole temperature measurements, the ERT/RST measurements and the application of the four-phase model resulted in an in-depth view of the investigated area, which is a major prerequisite for future modelling studies allowing for a better treatment of the present small-scale spatial ground variabilities.

1 Introduction

Permafrost in high-mountain areas occurs within different subsurface materials and textures. As the physical properties of the different materials will affect the thermal regime of

the permafrost in different ways, detailed knowledge about the active layer material and its seasonal changes is essential to understand the long-term impact of climatic changes on mountain permafrost. More precisely, the composition of the active layer material (grain size, porosity, ice/water content,

and the corresponding thermal and hydrological properties) as well as exogenous physical processes such as the infiltration of water or chemical and physical weathering play an important role.

During the last decades various geophysical methods have become a useful tool for characterizing the subsurface material in permafrost areas without disturbing it (e.g. Barsch, 1973; Fisch and Haerberli, 1977; Scott et al., 1990; Wagner, 1996; Vonder Mühll et al., 2001; Musil et al., 2002; Hauck et al., 2004; Maurer and Hauck, 2007; Kneisel et al., 2008). Electrical resistivity tomography (ERT) and refraction seismic tomography (RST) are two of the most common methods since they are both sensitive to phase change between frozen and unfrozen ground, but otherwise identified. As electric conduction takes place in the still unfrozen part, electrical properties remain sensitive to the amount of unfrozen water that can be present in permafrost material even at temperatures well below the freezing point. In contrast, the seismic P-wave velocity depends on the solid matrix and changes quickly with the aggregate change from water to ice and vice versa (Pearson et al., 1983). Consequently, changes in temperature can cause different behaviour of resistivities and seismic velocities. A combination of both methods can reduce the ambiguity in the interpretation (e.g. a field-based comparison of both methods is given by Otto and Sass, 2006, and Hauck and Kneisel, 2008a).

Within high-alpine permafrost research, geophysical soundings are primarily used for determining the spatial extent and distribution of permafrost occurrences (e.g. Lugon et al., 2004; Otto and Sass, 2006; Ribolini et al., 2010; Scapozza et al., 2011), as well as for analysing the internal structure and ice occurrences (e.g. Delaloye and Lambiel, 2005; Lambiel and Pieracci, 2008; Morard, 2011). Knowing the geophysical properties of periglacial material provides insight into thermal and hydrological processes such as spatial thaw and refreezing processes of permafrost rocks (Krautblatter et al., 2010) or enables the identification of water migration processes within landslide areas (Marescot et al., 2008). In addition, the geotechnical stability of thawing permafrost slopes partly depends on the same physical properties and their changes in time, leading to instabilities of engineering structures such as cable car pylons or avalanche protection structures (Phillips et al., 2007). The abovementioned studies are based on a qualitative interpretation of the ERT results for permafrost distribution; further steps would be a quantitative interpretation, for example for providing the percentage amount of ice and its changes in time. First approaches are given by Krautblatter et al. (2010), who interpreted temperature and stability relevant factors by calibrating ERT with frozen rock temperatures, and by Hauck et al. (2011), who used a four-phase model to calculate the volumetric fractions of the ground constituents.

Regularly repeated geoelectrical observations can be useful for detecting changing permafrost conditions as they allow for the identification of seasonal and annual changes in

the unfrozen water content. The ERT-monitoring (ERTM) technique has become an appropriate technique for observing temporal changes in the active layer, and has already been successfully applied within the last years (Hauck, 2002; Kneisel, 2006; Krautblatter et al., 2010; Ottowitz et al., 2011; Hilbich et al., 2011). In the year 2005, the first installation of a fixed ERTM network in permafrost was undertaken at different mountain permafrost sites in the Swiss Alps by the Swiss Permafrost Monitoring Network (PERMOS; Hilbich et al., 2008a). A recently performed monitoring study by Roedder (2012) emphasized its suitability for gaining deeper insights into ground thermal and hydrological processes within periglacial materials. Even short-term processes such as the spring zero curtain could be observed, indicating the infiltration of snow melt water by a very rapid response in resistivity (Hilbich et al., 2011; Roedder, 2012). In further studies, the spatial distribution of freezing processes within a talus slope (Morard, 2011) or the freeze–thaw weathering in bedrock (Rode and Sass, 2011) could be observed by repeated ERT.

An extensive analysis of borehole temperature data of different periglacial materials in the high-alpine permafrost area Murtèl–Chastelets in the eastern Swiss Alps by Schneider et al. (2012) recognized a need for the following: (i) more information about the subsurface material and composition to understand the spatial and temporal varying processes occurring in high-alpine permafrost regions, and (ii) a detailed analysis of the response of different permafrost materials to changing atmospheric variables (such as temperature and snow).

Thus, the aim of this work is (i) to characterize the subsurface material of the same investigation area by combined boreholed temperature data, ERT and RST measurements, (ii) to show the variability of geophysical properties on a small spatial range and (iii) to provide data for the validation and initialization of physically based models.

For that purpose, a systematic ERT monitoring (ERTM) analysis was performed from 2009 to 2012 in addition to temperature data measurements. The application of the same configuration, monitoring interval and inversion parameters for each measurement allowed for reducing potential errors due to non-climatic factors such as inversion artefacts, and provided reliable information about processes within the ground material and its composition. In addition, the application of a four-phase model, which is based on the geophysical data, allowed for a detailed description of the subsurface.

2 Data acquisition and processing

2.1 Investigation site

The study area is situated in the Upper Engadine (eastern Swiss Alps) at a height of approximately 2600 m a.s.l. (46°26' N, 9°49.5' E; Fig. 1). As it is part of the “inner Alpine province”, the area receives little precipitation and

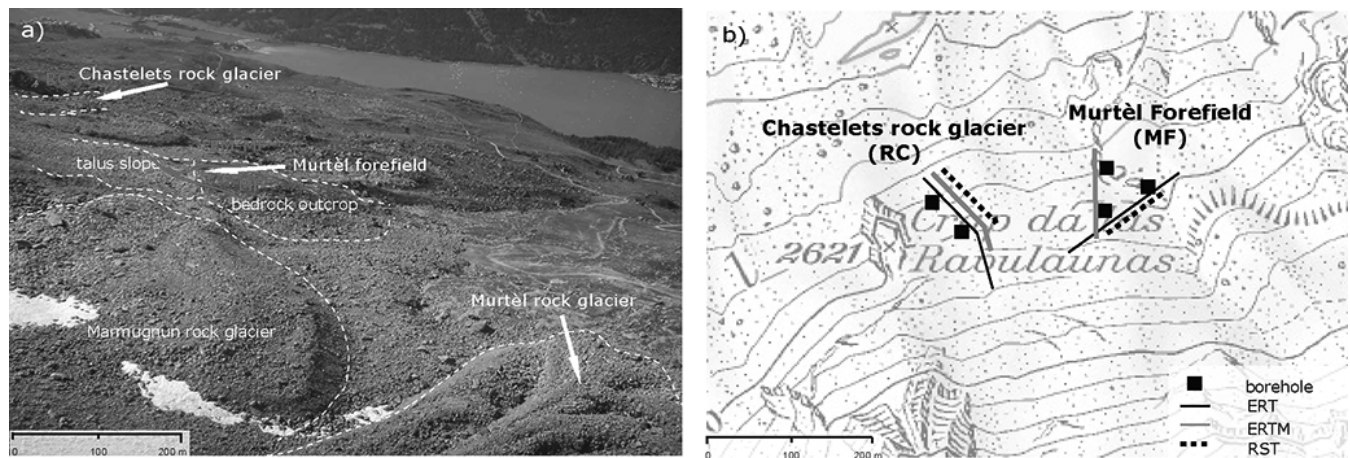


Figure 1. Area of investigation, Murtèl–Corvatsch, eastern Swiss Alps. (a) Photograph including the geomorphological features and the position of the geophysical profiles (red lines), and (b) topographical map with marked positions of the five boreholes (Hanson and Hoelzle, 2005) and detailed position of the ERT (black), ERTM (grey) and RST (black dotted) profiles.

high incoming solar radiation. The local microclimate during summer is characterized by strong, moist afternoon winds originating from the Italian plains to the west (“Malojawind”). The mean annual air temperature (MAAT) is about -1.8°C and the average snow cover is 1.4 m (Schneider et al., 2012). As indicated in Fig. 1a, the area comprises several periglacial features such as rock glaciers and talus slopes, which are surrounded by a steep northwest-facing rock wall. Beside the Murtèl rock glacier, which is the most prominent geomorphological feature of the area, further rock glaciers such as the Chastelets and the Marmügnun rock glacier have developed. For the Murtèl rock glacier comparatively low creep rates of 5 to 15 cm a^{-1} were determined at the surface (Kääb et al., 1998). An assemblage of fossil landforms (cf. Fig. 1a, the partly vegetated deposits in front of the rock glaciers) indicate the already long-persisting geomorphological dynamics of this area. The parent rock material of the area was determined as granodiorite and metamorphosed basalt of the Corvatsch nappe as well as muscovite and calcite marble of the Chastelets series (King et al., 1987). The area belongs to one of the best-investigated permafrost areas in the Swiss Alps to date (e.g. Haeberli et al., 1988; Hoelzle et al., 2002; Hanson and Hoelzle, 2005; Maurer and Hauck, 2007), and is part of the PERMOS network (Permafrost Monitoring Switzerland, Noetzli and Vonder Mühll 2010). It is equipped with a micrometeorological station (Hoelzle and Gruber, 2008), a borehole network of seven boreholes and three ERT-monitoring profiles. The positions of the used boreholes and ERT profiles are indicated in Fig. 1b.

2.2 Ground temperatures

In order to observe changes in ground temperature, a shallow borehole network was installed in 2002 within the study area (Hanson and Hoelzle, 2005). The boreholes were placed

within the forefield of the Murtèl rock glacier and within the Chastelets rock glacier, which is situated to the west of the Murtèl rock glacier (cf. Fig. 1). One borehole was drilled in bedrock (Bb), one was placed on a coarse blocky talus slope (TSc), one was drilled into the fine-grained material of the Chastelets rock glacier close to its front (RCf) and the last one was located in the coarse blocky part of the Chastelets rock glacier (RCc) (Fig. 1b). Each borehole has a depth of 6 m and is equipped with 18 thermistors placed at 0.1, 0.2, 0.3, 0.4, 0.5, 0.6 and 0.8 m, every 0.5 m from 1 to 5 m and at 6 m depth.

2.3 Geophysical measurements

2.3.1 Electrical resistivity tomography (ERT)

The application of ERT in permafrost regions is based on determining the varying electrical conductivity ($= 1/\text{resistivity}$) of the subsurface, composed of bedrock, sediment, air, ice and water. Applying an electric current into the ground through two electrodes, the resulting potential difference between two other electrodes along the same profile line consisting of many electrodes was measured. The apparent resistivity ρ_a could then be calculated as a function of the current, the voltage and a geometric factor depending on the geometry of the electrodes. A two-dimensional distribution of apparent resistivities could be obtained by repeating this procedure along an electrode array for different four-electrode combinations depending on the chosen configuration (Wenner, Wenner–Schlumberger, dipole–dipole; Reynolds 2005).

A 2-D model of the specific resistivity ρ_s distribution was calculated from the measured apparent resistivity data ρ_a by an iterative tomographic inversion process (software RES2DINV, Loke, 2011). This program calculates the tomographic inversion model by using an iterative least-squares

method (deGroot Hedlin and Constable, 1990; Loke and Barker, 1996). Both, the inversion approach and the software Res2dinv are well tested and have been successfully applied to high-alpine permafrost terrain, such as the Murtèl rock glacier (Hauck et al., 2003; Hauck and Vonder Mühl, 2003; Hilbich et al., 2009).

Two ERTM profiles covering different subsurface materials were installed in 2009. An ERTM includes a fixed electrode array, which is permanently connected via cables to an adapter box at which a resistivity meter can be connected (described in detail by Hilbich et al., 2008b). To calibrate the indirect geophysical measurements with direct temperature measurements, each profile passes two boreholes (Fig. 1b). The subsurface material of profile EM-MF passes from bedrock to a talus slope. The profile EM-RC is placed on the Chastelets rock glacier, containing fine-grained and coarse blocky material (Fig. 1a). The measurements were conducted using a Syscal Junior/R1 (IRIS instruments). The profiles consist of 48 electrodes (EM-MF) and 72 electrodes (EM-RC) with a small electrode spacing of 1 m in order to yield a high resolution. The presented ERTM data were measured in a bimonthly interval using the Wenner configuration.

An appropriate choice of inversion parameters is required to obtain reliable features within the inversion model. For example, the regularization parameter λ specifies the weighting between data constraints and a priori information. As default, RES2DINV reduces the value of λ by 50 % for each subsequent iteration until a user-specific minimum value λ_{\min} is reached (Loke, 2011). Although small λ_{\min} values tend to over fit the data and artefacts can subsequently result from the inversion (Hauck et al., 2003), a minimum smoothness was applied in order to avoid the suppression of small-scale variability, potentially present along the profile lines. Care therefore has to be taken to not over-interpret the results. The robust scheme (L1-norm) was applied to invert the ERTM data as it models more accurately the observed changes in resistivity and to avoid an over-smooth spatial representation which a least-square constraint scheme may cause (Hilbich et al., 2008b).

To calculate mean resistivity values for the different materials (bedrock, coarse blocky, fine-grained) and depths, sections of 20 to 40 neighbouring measurement points were extracted from the inversion model (cf. red rectangles marked as an example within the first tomogram of the Figs. A1 and B1 in the Appendix). For all data sets the same depth levels were used as they are specified by the inversion grid.

2.3.2 Refraction seismic tomography (RST)

refraction seismic measurements allow for the differentiation between frozen and unfrozen materials, as the seismic P-wave velocity (V_p) changes with variations in the ice/water content. Where the resistivity contrast between ice, air and certain rock types is small, refraction seismic surveys provide a large contrast between very slow velocities in air

and high velocities in pure ice (Hauck and Kneisel, 2008b). But as V_p has a wide range for permafrost materials (ranging from around 2500 to 4200 m s^{-1} , Hauck and Kneisel, 2008b) and has an overlap for permafrost ice and bedrock between 2000 and 6000 m s^{-1} depending on the rock type (Hecht, 2000), the differentiation of the subsurface material and composition is difficult, especially within talus slopes and rock glaciers. Assuming that lithospheric conditions of the subsurface (material composition and texture) are stable, even small changes of V_p can indicate zones with significant changes in ice content, which allows for the detection of the active layer–permafrost boundary (permafrost table) and observation of seasonal and annual changes in the ice content (Hilbich, 2010).

The RST measurements were conducted using a Geode instrument (Geometrics) with 24 geophones. The seismic signal was generated by a sledge hammer, beaten on a boulder or a steel plate. The spacing of the geophones was 2 m and the shot positions were placed at the midpoint between the geophones. Off-end shots were performed between 2 and 8 m distance from the last geophone at each site. To obtain an adequate signal-to-noise ratio, 10–20 shots were stacked at each shot point. The RST profiles (S-RC and S-MF) were conducted at coincident locations with the ERTM profiles (Fig. 1) and were carried out once a year (2009–2012, each in August).

The data processing and the calculation of a 2-D velocity model (first arrival picking, travel time analysis and tomographic inversion) was done by using the software REFLEXW 6.0 (Sandmeier, 2010). The inversion is based on the SIRT algorithm (simultaneous iterative reconstruction technique), which adapts iteratively the synthetic travel times (calculated by iterative forward modelling) to the observed travel times. For each profile the same initial model and the same model parameters were applied for all measurements.

2.3.3 Estimation of the volumetric fractions of ice, water and air

Based on the 2-D tomographic electrical and seismic measurements, a four-phase model (Hauck et al., 2011) was applied to quantify the volumetric fractions of ice, water and air. Since the model depends on a prescribed porosity, the volumetric fractions are a function of the available pore space. In the model it is assumed that each cell of the 2-D model domain consists of the sum of the volumetric fractions for rock f_r , liquid water f_w , ice f_i and air f_a . For each model block the equation

$$f_w + f_r + f_i + f_a = 1 \quad \text{with} \quad 0 \leq f_w, f_r, f_i, f_a \leq 1 \quad (1)$$

must be fulfilled. To determine the specific fractions, the model is further based on two well-known petrophysical relationships: Archie's second law and an extended Timur equation. Archie's second law relates the resistivity ρ (in Ωm) of a three-phase medium (rock matrix, liquid, air-filled pore

space) to the resistivity of the pore water ρ_w , the porosity Φ and the saturation – that is the fraction of the pore space occupied by liquid water S_w :

$$\rho = a\rho_w\Phi^{-m}S_w^{-n}, \quad (2)$$

where a , m and n are empirically determined parameters (Archie, 1942). The model holds for partly frozen material of moderate temperatures below zero (Hauck, 2002). The porosity and the saturation can be expressed through the volumetric fractions introduced in Eq. (1) using

$$\Phi = 1 - f_r$$

$$S_w = \frac{f_w}{\Phi} = \frac{f_w}{1 - f_r}. \quad (3)$$

Timur's equation relates seismic P-wave velocities to the porosity and ice content of the material (Timur, 1968). An extension of Timur's equation to four phases enabled the model to take unsaturated conditions into account. The equation states that the reciprocal of the P-wave velocity (the so-called slowness) of a mixture, $1/v$, is equal to the sum of the slownesses of the respective components, each weighted by its volumetric fraction (Hauck et al., 2011):

$$\frac{1}{v} = \frac{f_w}{v_w} + \frac{f_r}{v_r} + \frac{f_i}{v_i} + \frac{f_a}{v_a}. \quad (4)$$

Though the model does not hold for sediments with a considerable amount of clay particles, it has been assumed that this parametrization is a fair approximation for the heterogeneous conditions in Alpine permafrost terrain (Hauck et al., 2011). As a constant porosity model probably oversimplifies the heterogeneous ground conditions, a spatially variable, material-dependent porosity was implemented. In addition, a porosity decrease with depth was assumed, which was individually adapted to the various materials. To simulate the large air-, water- or ice-filled voids between the boulders of the rock glacier, a porosity of 50% was chosen for coarse blocky material. For the other materials an initial porosity of 30% (fine-grained material) and 15% (bedrock) was assumed. To reduce the number of degrees of freedom of the model, fixed values were used for the Archie parameters a , m , and n throughout the whole model grid. An overview of the used model parameters is presented in Table 1. Further details regarding the four-phase model including a test study from the Murtèl rock glacier are given in Hauck et al. (2011).

3 Results

3.1 Chastelets rock glacier

The mean annual temperatures, measured in the two boreholes (RCc and RCf) along the seismic and electric profiles (E-RC and S-RC) give evidence that the Chastelets rock glacier has a permanently frozen regime with temperatures

Table 1. Model parameters of the four-phase model used in this study. The values are in accordance with King et al. (1988), Hauck and Kneisel (2008b) and Hauck et al. (2011). The porosity Φ expresses the value at the surface for each material, whereas $\Delta\Phi$ is the material-dependent depth gradient in [% m⁻¹].

parameter	site	value
a		0.7
m		1.6
n		2
v_w [m s ⁻¹]		1500
v_i [m s ⁻¹]		3500
v_a [m s ⁻¹]		330
v_r [m s ⁻¹]		6000
ρ_w [Ω m]		100
Φ_c	RCc, TSsc	0.5
Φ_b	Bb	0.15
Φ_s	RCf	0.3
$\Delta\Phi_c$ [% m ⁻¹]	RCc	2.08
$\Delta\Phi_s$ [% m ⁻¹]	TSsc	3.3
$\Delta\Phi_b$ [% m ⁻¹]	Bb	0.3
$\Delta\Phi_s$ [% m ⁻¹]	RCf	0.42

< 0 °C below the active layer (Fig. 2c, d). While the sediment (RCf) site shows a thermal regime close to 0 °C, the permafrost body of the rock glacier (RCc) has an annual mean temperature around -1 °C. The active layer depth is approximately 3.5 to 4 m for RCf and has a high annual variability, as shown in Schneider et al. (2012). In contrast, the active layer depth of the rock glacier remains constant each year at 2.5 to 3 m depth. The ground surface temperatures (GST) vary from -4.5 (winter mean) to 8.6 °C (summer mean).

In August 2009 joint ERT and RST measurements were performed at the Chastelets rock glacier. The ERT profile (RC) presented in Fig. 3a shows in the upper and central part a near-surface layer with strongly varying resistivity values in the range of 5–20 k Ω m and a layer with remarkably high resistivities of 20–50 k Ω m below. The high-resistive layer has a thickness of approximately 10 m. The lowest values (1–2 k Ω m) were found in the lower part of the profile within the fine-grained sediment (RCf) at the frontal part of the rock glacier. At greater depths (> 6 m), the values increase up to approximately 6 k Ω m. Pursuant to the ERT profile, the RST profile (Fig. 3c) shows low P-wave velocities of around 750 m s⁻¹ within the sediment part and close to the surface. The P-wave velocities within the coarse blocky rock glacier part are continually increasing up to 3200 m s⁻¹ at 9.5 m depth. In contrast only low and slightly increasing P-wave velocities with depth (up to 2000 m s⁻¹) were found at the front of the rock glacier.

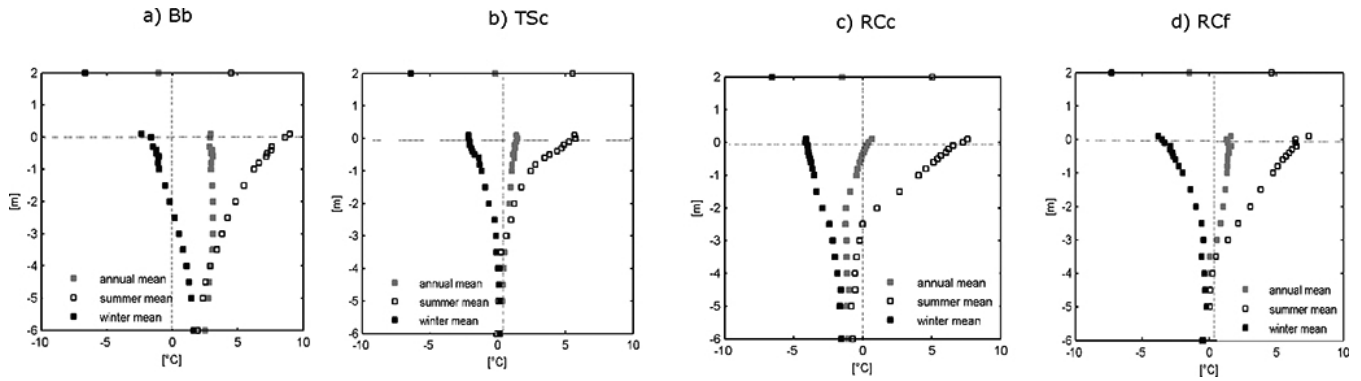


Figure 2. Mean annual (grey) and mean seasonal (summer – white; winter – black) temperatures for each borehole and depth from 2002 to 2010 (taken from Schneider et al., 2012). The summer season was determined as the time between the end of the spring zero curtain and the first time when the daily mean air temperature drops below 0 °C. The winter season was characterized by a snow cover of more than 0.3 m and a daily mean air temperature below 0 °C.

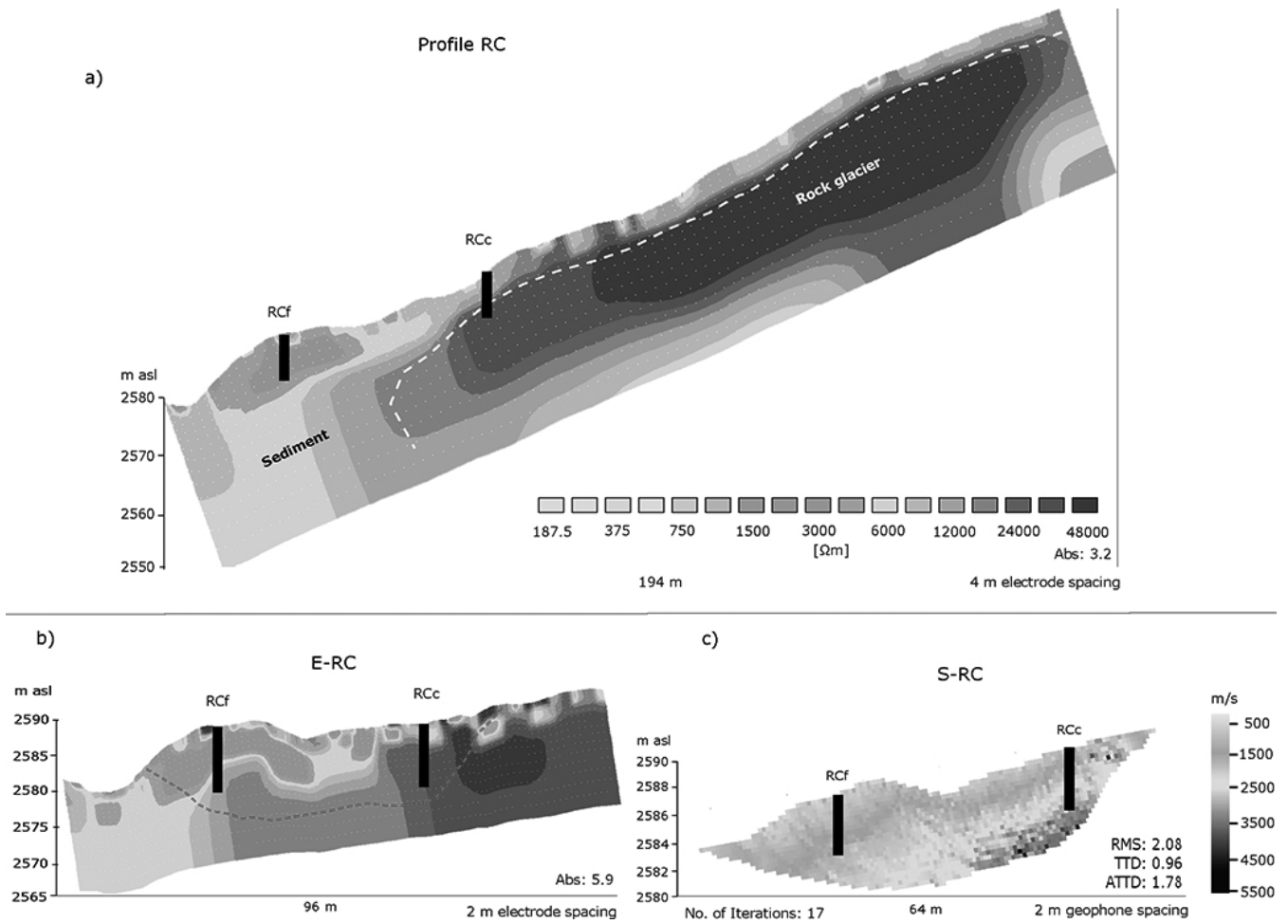


Figure 3. ERT and RST profiles of the Chastelets rock glacier. The black bars mark the positions of the boreholes in the fine-grained part (RCf) and in the coarse blocky part (RCc). (a) ERT profile measured in August 2010 with 4 m electrode spacing. The white line marks the interpreted transition between the unfrozen part and the permafrost ice. (b) ERT (E-RC) and RST (S-RC) profiles measured in August 2009 and used for the four-phase model calculations. The red line marks the location of the RST profile. The model uncertainties are indicated as follows: Abs = absolute error, RMS = root mean square, TTD = total time difference [m s^{-1}], ATTD = absolute total time difference [m s^{-1}].

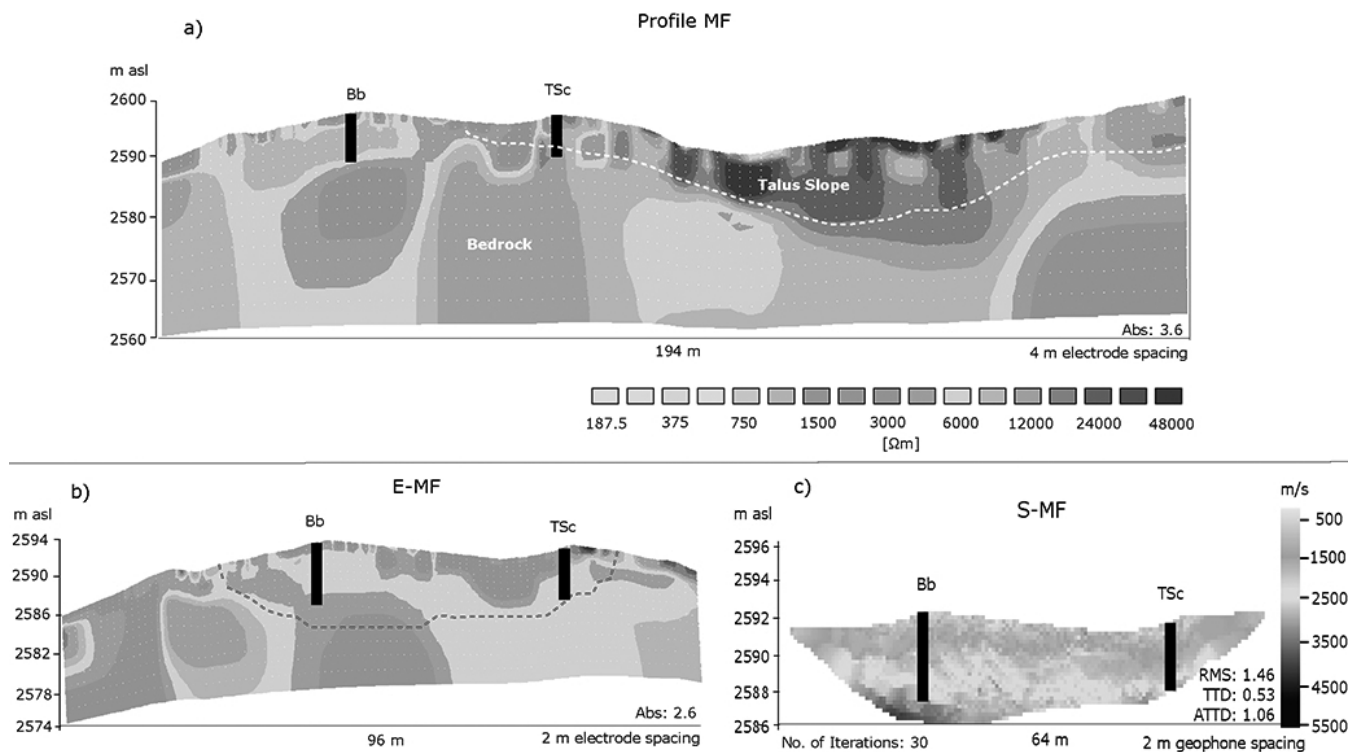


Figure 4. ERT and RST profiles of the Murtèl forefield measured in August 2009. The black bars mark the positions of the boreholes in the bedrock (Bb) and talus slope (TSc). **(a)** ERT profile measured with 4 m electrode spacing. The white line refers to the spatial extension of the talus slope. **(b)** ERT (E-MF) and RST (S-MF) profiles used for the four-phase model calculations. The red line marks the location of the RST profile. The resistivity scale bar is valid for both ERT profiles. The model uncertainties are indicated as follows: Abs = absolute error, RMS = root mean square, TTD = total time difference [m s^{-1}], ATTD = absolute total time difference [m s^{-1}].

3.2 Murtèl forefield

The borehole temperature data of the Murtèl forefield revealed that the talus slope site (TSc) has a permanently frozen regime with temperatures $< 0^\circ\text{C}$ below the active layer (Fig. 2b). In contrast, the bedrock site (Bb) shows only seasonal frost (Fig. 2a). The mean active layer depth is 4 m for TSc and has a high annual variability as shown by Schneider et al. (2012). The GST varies from 5.7°C (TSc) to 9.2°C (Bb) during summer and reaches a wintery mean of -2.2°C for both sites.

In August 2009 joint ERT and RST measurements were performed at the Murtèl forefield. The ERT tomogram presented in Fig. 4a displays resistivity values between 3 and $7\text{ k}\Omega\text{m}$ for the part of the profile, where the bedrock is visible at the surface. At the talus slope strong variations in resistivity, in the range of $6\text{--}50\text{ k}\Omega\text{m}$, occur within the uppermost 8 m. The resistivity values below 8 m depth reach $6\text{--}7\text{ k}\Omega\text{m}$ and are therefore in the range of the values found for the bedrock. The low-resistive areas with about $2\text{ k}\Omega\text{m}$ at the lower right corner of the 2-D image (Fig. 4a) have to be interpreted with care, since inversion artefacts might be present in these areas due to the lateral extrapolation of the inversion model (an extended model grid was cho-

sen; Loke and Barker, 1996). The P-wave velocities of S-MF reach a maximum of 3.5 km s^{-1} within the firm bedrock part (Fig. 4c). Similar velocities were found at larger depths within the talus slope area. Within the uppermost 3 m, values about 1.5 km s^{-1} were measured along the whole profile, whereas the lowest values (down to 500 m s^{-1}) were found close to the surface.

3.3 Four-phase model results

Based on the ERT and RST data of the Chastelets rock glacier, the volumetric fractions of water, air and ice were calculated by the four-phase model (Fig. 5, left panel). For the rock glacier body an ice content of approximately 30 % was calculated, which corresponds to 60 % ice saturation for a model porosity of 50 %. In addition, an ice content of approximately 25 % was modelled in the central part of the profile (around 1020 m horizontal distance). As the electrode coupling was difficult at this place, artefacts might be produced by the geoelectric inversion process, leading to an overestimation of the absolute ice content by the four-phase model. The values around 1020 m horizontal distance should therefore be interpreted with care. Further, a water content close to 0 % was modelled in all cases except for a small

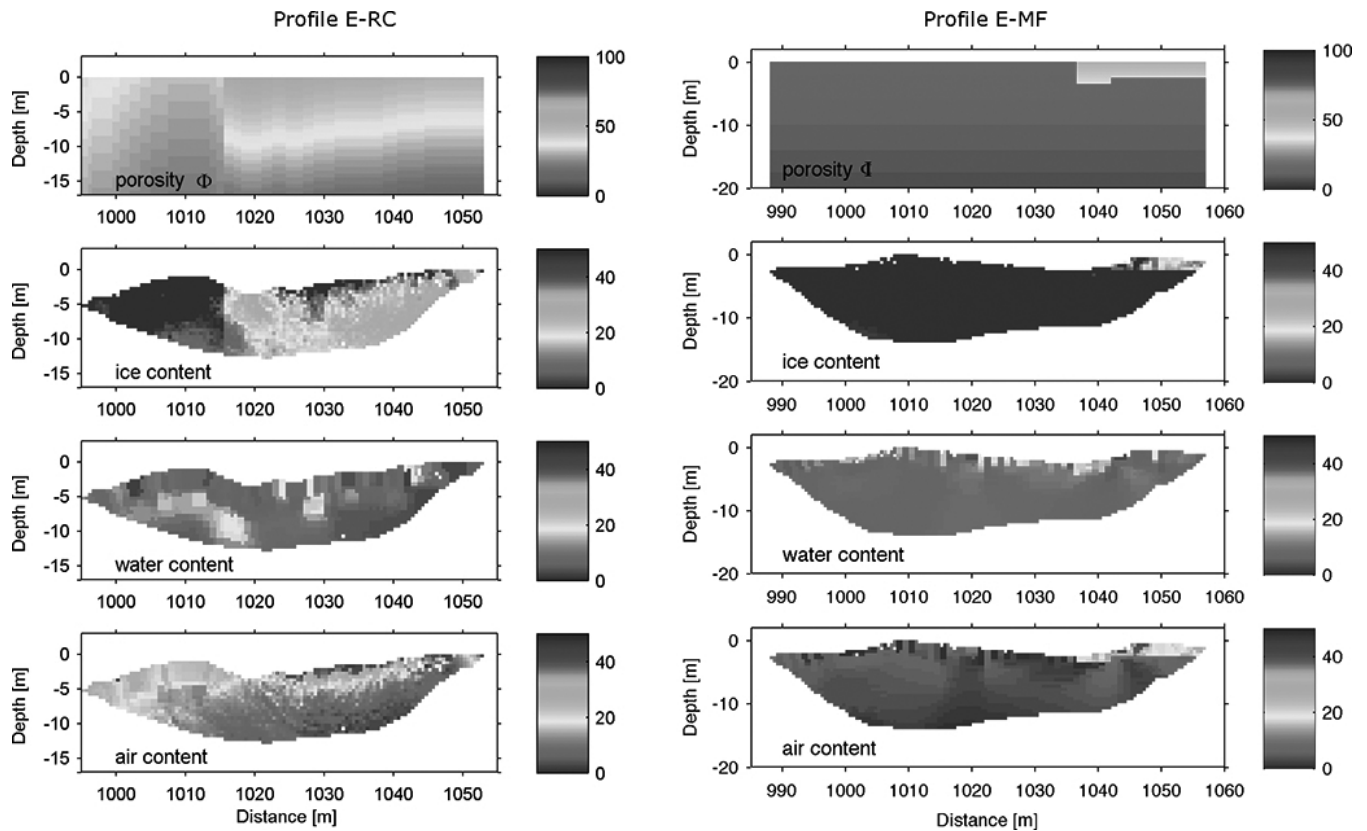


Figure 5. Four-phase model results for the Chastelets rock glacier (E-RC) and the Murtèl forefield (E-MF). Calculated with a material-dependent porosity gradient. The porosity decreases with depth as follows – Bb: $0.3\% \text{ m}^{-1}$; TSc: $3.3\% \text{ m}^{-1}$; RCc: $2.08\% \text{ m}^{-1}$; and RCf: $0.42\% \text{ m}^{-1}$.

anomaly at the horizontal distance 1029 m. In dependence on the prescribed porosity, the air content decreases quickly with depth.

Within the fine-grained sediment no ice content was calculated, but an increased water content up to 15 % was found below 4 m depth. Although the prescribed porosity at 5 m depth is lower than within the coarse blocky part, a higher absolute air content (up to 30 %) was calculated.

Within the MF profile (Fig. 5, right panel), almost homogeneously distributed volumetric fractions of ice, water and air were determined, except for the upper 3 m. All but no ice content and a water content of $\sim 10\%$ were modelled. Surprisingly, a strongly varying absolute water content with values up to 20 % was found close to the surface. The blocky layer of the talus slope, which was modelled with an initial porosity of 50 %, shows a mean absolute air content of 25 % and a mean absolute ice content up to 25 %. As the summer borehole temperatures are above 2°C , the ice content is probably overestimated by the four-phase model due to the high resistivity values of the ERT data set at the surface of the talus slope (cf. Fig. 4b).

3.4 Seasonal changes

Seasonal changes in resistivity were analysed from the bi-monthly ERTM measurements during the years 2009 to 2012 along the profiles at Murtèl forefield (EM-MF) and Chastelets rock glacier (EM-RC) and are summarized in Figs. 6 and 7. The complete ERT tomogram series for both profiles are presented in the Appendix (Figs. A1 and B1). Figure 6 shows the resistivity values as depth profiles, grouped by material, which illustrates the seasonal behaviour of resistivity for the different materials. In general, the ERT monitoring series of the Chastelets rock glacier (EM-RC, including RCc and RCf) shows a stronger seasonal variability in specific resistivity than the EM-MF monitoring series. By analysing the variability of each material, it can be seen that the seasonal changes are larger for RCc ($\sim 30 \text{ k}\Omega\text{m}$) than for RCf ($\sim 4 \text{ k}\Omega\text{m}$), and smaller for the Murtèl forefield sites.

In both ERTM series, the strongest seasonal variations occurred within the uppermost 3 m, with increased resistivities during winter up to $250 \text{ k}\Omega\text{m}$ (RCc) and $70 \text{ k}\Omega\text{m}$ (Bb), respectively (Figs. 6, B1 and A1). The resistivity values in the lower part of the talus slope as well as in the bedrock part varied between 5 and $8 \text{ k}\Omega\text{m}$. The increasing values in the left part of the profile (Fig. A1) should not be taken into account,

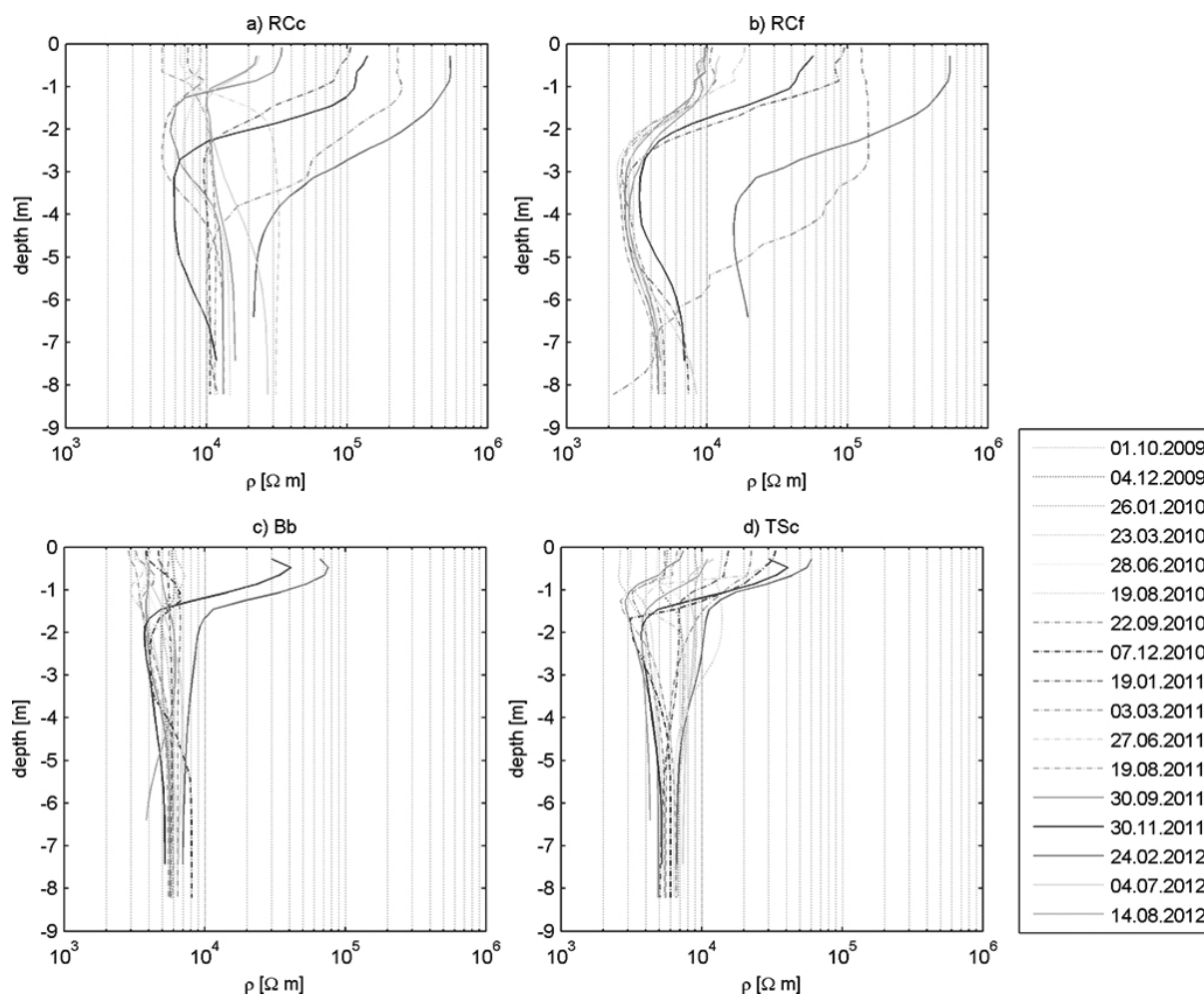


Figure 6. One-dimensional mean vertical sections of specific resistivity for different materials. Measurements were taken in bimonthly intervals from August 2010 to August 2011 (for **a** and **b**) and from October 2009 to August 2012 (for **c** and **d**), respectively. The values were extracted from the inversion models and calculated as a mean of 20–40 values for each material and depth (bedrock (Bb), talus slope (TSc), rock glacier fine-grained (RCf) and rock glacier coarse blocky (RCc)). The individual tomograms are shown in the Appendix for reference.

as the inversion routine tends to create artefacts at the edge of the profile or the values might be influenced by lateral effects due to the surface topography. The bedrock site (Bb) showed in general only small seasonal variations, and predominantly within the upper 2 m (Figs. 6c and 7). Remarkably high values were found close to the surface during winter 2011/2012 (Fig. 6c).

In Fig. 8 the ERT data, the snow height and the air temperature are shown for the entire observation period. During summer, the resistivity values remain around 7 (Bb, TSc) and 10 kΩm (RCc, RCf), respectively. At all sites, elevated resistivity data were found during the winter months, while at the Chastelets rock glacier the values increase much more than at the Murtèl forefield. The highest values were measured during winter 2011/2012, which coincide with the smallest amount of snow (~0.5 m, compared to the other years when a mean snow height of 1 m was measured, cf. 8). Within all

3 yr, an annual temperature range from -22 to 14°C was measured.

4 Discussion

4.1 Chastelets rock glacier

Within the active layer of the Chastelets rock glacier, P-wave velocities of 1500 m s^{-1} (Fig. 3) were determined, indicating the presence of loose boulders and a high amount of air-filled pore space (Hauck and Kneisel, 2008b). Likewise, Maurer and Hauck (2007) and Roedder (2012) found seismic velocities $< 2000\text{ m s}^{-1}$ for the coarse blocky active layer of the adjacent Murtèl and Rabgiusa rock glacier.

Below the active layer ($> 3\text{ m}$ depth), temperatures around -1°C (Fig. 2c), P-wave velocities up to 3500 m s^{-1} and the resistive anomaly of approximately $30\text{ k}\Omega\text{m}$ (Fig. 3) confirm a permafrost occurrence of 10–15 m thickness within

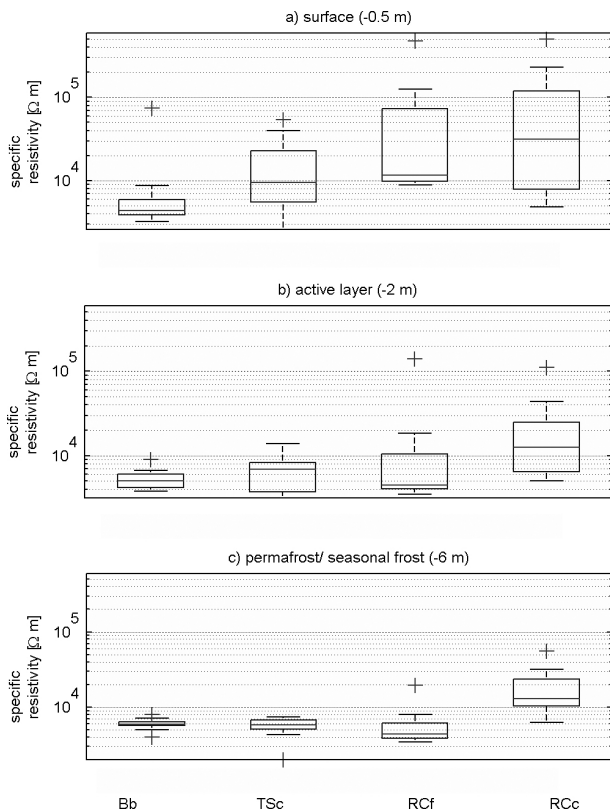


Figure 7. Seasonal changes in specific resistivity taken from the inversion models for different materials and for three different depths. The box plots contain 18 measurement periods (Bb and TSc) and 11 measurements periods (RCc and RCf) derived within the years 2009 to 2012. The ERT values were extracted from the inversion tomograms and calculated as mean of 15–40 values for each site and depth.

the Chastelets rock glacier. Based on commonly used interpretations of resistivity on rock glaciers, 30 kΩm is not an indication of ice-rich conditions. For this usually values > 100 kΩm are found (Hauck and Kneisel, 2008b). Hauck and Vonder Mühl (2003) observed resistivity values up to 1–2 MΩm at the nearby Murtèl rock glacier, where various studies confirmed the presence of massive ice (e.g. Haerberli et al., 1988; Vonder Mühl and Holub, 1992; Vonder Mühl and Klingele, 1994; Hoelzle et al., 2002; Arenson and Springman, 2005). In addition, two other field studies in the vicinity of the Chastelets rock glacier revealed similar temperature and resistivity values. One was undertaken at the Muragl glacier forefield, and resistivity values about 30 kΩm were detected within the permafrost body. Kneisel (2006) interpreted these values as permafrost material which is rich in unfrozen water with frozen marginal parts. Observations at the nearby Rabgiusa rock glacier revealed resistivity values of 10 to 300 kΩm at temperatures close to the melting point (−0.5 °C at 5 m depth; Roedder and Kneisel, 2012). All three investigations suggest the occurrence of discontinuous

permafrost which is highly sensitive to increasing air temperatures (Maurer and Hauck, 2007).

The results of the four-phase model (Fig. 5, left panel) confirm an ice content of maximum 35 % and a maximum water content of 5 % within the rock glacier body. This corresponds almost to full ice saturation, with prescribed porosity of 40 %, and agrees with the values found for the Murtèl rock glacier (50 %) and the Muragl rock glacier (45 %), which were modelled with a porosity of 50 % (Hauck et al., 2011).

The seasonal changes in resistivity within the permafrost body of the Chastelets rock glacier are in a range of ~ 15 kΩm (Figs. 6a and 7c, RCc). These values would indicate seasonal varying changes in the unfrozen water content within the rock glacier, which we estimate to be probable, as the virtual borehole sections were taken from the upper 8 m and close to the front of the rock glacier (Fig. 3).

The small and only slightly increasing P-wave velocities with depth within the fine-grained sediment indicate the presence of uncompacted material. Further, a conspicuously low-resistive anomaly of 2–4 kΩm is present between 2 and 5 m depth (Figs. 3 and 6b). The four-phase model calculated an increased water content up to 15 % below 3 m depth at a prescribed porosity of 25 % (Fig. 5, left panel). To retain this water content, an impermeable matrix such as bedrock or a frozen layer has to exist below. The calculations of the four-phase model point to the fact that a frozen layer is present below 7 m depth, as increased ice content of ~ 10 % was determined (Fig. 5). Furthermore, it is surprising that the seasonal changes in resistivity within the fine-grained sediment are lower than within the coarse blocky material. In the case of higher water content, more water would be available for freezing coinciding with strongly increasing resistivities. This indicates that not all liquid water freezes during winter, but a certain amount of conductive, unfrozen water remains within the fine-grained material even at temperatures < 0 °C.

4.2 Murtèl forefield

The survey within the Murtèl forefield covered bedrock (Bb) and a talus slope (TSc). Whereas only seasonal frost was detected for Bb, the talus slope showed a permanently frozen regime beneath 3.5 m depth with temperatures close to 0 °C (Fig. 2a, b).

The small seasonal changes in resistivity beneath 2 m depth within the bedrock indicate homogeneous material and a stable aggregate state during the year. Within the uppermost 2 m, low P-wave velocities and seasonal changes in resistivity up to 4 kΩm were found (Figs. 4c and 7b). This might indicate weathered bedrock with a higher porosity (i.e. clefts) in the upper part. Weathering processes due to annual freeze–thaw cycles can reach a depth of more than 5 m (Matsuoka et al., 1998) and can cause an increase in porosity and a widening of the clefts (Hasler et al., 2012). Krautblatter (2008) showed that an increase of 10 % in porosity (air-filled pores) can reduce the P-wave velocity by 50 %

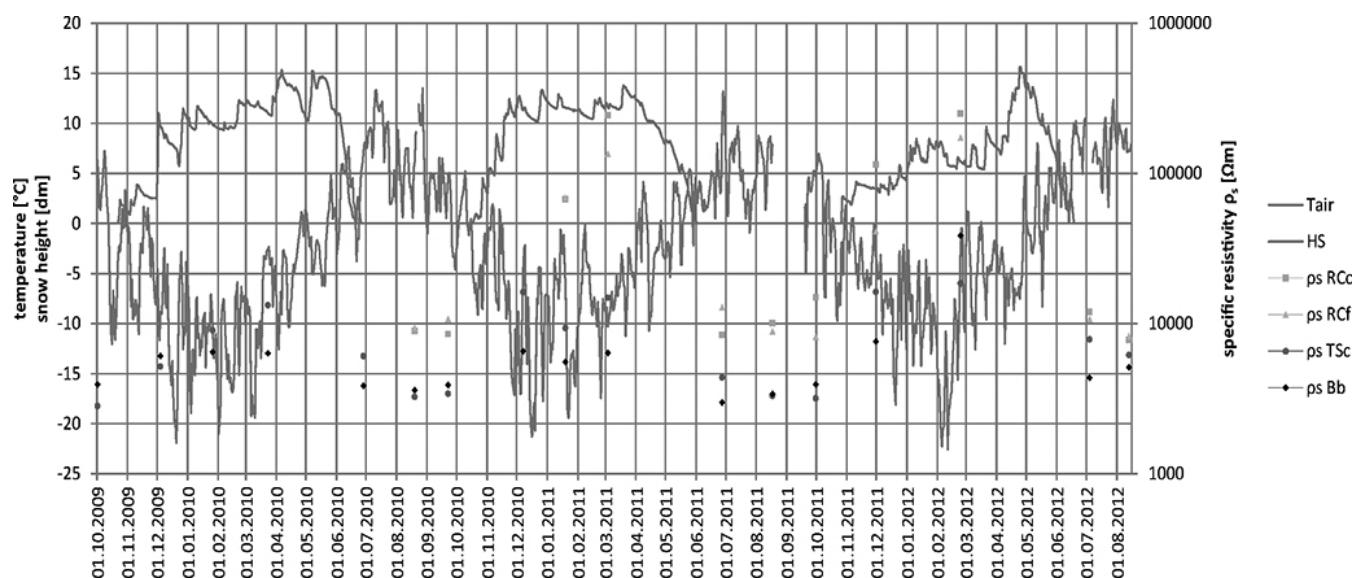


Figure 8. Daily mean snow height and air temperature measured at the micrometeorological station of the Murtèl rock glacier as well as (spatially) mean specific resistivity values for the different materials from 1 October 2009 to 15 August 2012. The mean specific resistivity values were taken from the repeated ERT measurements. Note that for RCc and RCf, the ERT measurements did not start before 19 August 2010.

within metamorphic rocks. At 10 m depth P-wave velocities of 2800 m s^{-1} were determined, which agree well with the values of 2600 m s^{-1} found for weathered bedrock (gneiss) (Jongmans et al., 1998). For unweathered samples (granodiorite) collected at the field sites, P-wave velocities of 3600 m s^{-1} were measured.

The low resistivity values close to the surface (Fig. 6c) may indicate an elevated water content within cracks of the weathered bedrock. Quasi-saturated conditions were determined by the four-phase model (Fig. 5, right panel), which calculated an absolute water content up to 15–20 % with prescribed porosity of 20 % close to the surface. However, this confirms the influence of weathering processes and the possible infiltration of meltwater within the bedrock material.

The talus slope exhibited rather low resistivity values ($\sim 7 \text{ k}\Omega\text{m}$) and low P-wave velocities (500 to 1500 m s^{-1}) within the active layer. Other RST surveys on talus slopes, which revealed values of around 1000 m s^{-1} , were interpreted as uncompacted material with huge amounts of air-filled pore spaces (e.g. Otto and Sass, 2006; Hilbich, 2010).

Below 3 m depth the P-wave velocities increase up to $\sim 3000 \text{ m s}^{-1}$. In consideration of the fact that the adjacent weathered bedrock exhibits velocities of $\sim 2800 \text{ m s}^{-1}$, it is possible that the blocky layer of the talus slope is followed by bedrock at 3 m depth. On the other hand, the measured values lie within the lower range of permafrost material (2450 – 4250 m s^{-1} , Hauck and Kneisel, 2008b). In combination with borehole temperatures below 0°C , a low ice content, for example in the form of ice-filled clefts, cannot be excluded. Musil et al. (2002) interpreted the P-wave velocities from 3000 to 4300 m s^{-1} measured at the rock glacier Muragl as

ice-cemented boulders. Hilbich (2010) found values up to 3500 m s^{-1} for a permafrost site (Schilthorn) consisting of strongly weathered dark limestone schists with little ice content below 5 m depth. However, the four-phase model does not confirm the presence of ice-filled clefts within the investigated area (cf. Fig. 5). Additional surveys with larger geophone spacing, enabling a greater depth of investigation, would be helpful for estimating the ice content more accurately. Likewise, RST measurements during winter would be useful to detect the seasonal changes in the ice content, but could not yet be performed because of the high snow cover and the prevailing avalanche danger.

Though the talus slope is very close to the bedrock site (the boreholes are at 25 m distance), the talus slope shows a permafrost regime below 4 m depth, while the bedrock exhibits only seasonal frost. This leads to the assumption that the coarse blocky buffer layer above the bedrock, in addition to lateral effects from the internal circulation of the talus slope above, provoked a thermal regime which is able to sustain the permafrost beneath.

4.3 Seasonal variations in specific resistivity

At all sites, the strongest seasonal variations in resistivity occurred within the uppermost 2–3 m (Figs. 6 and 7). In general, high variations at the surface (0.5 m, Fig. 7a) have to be interpreted with care, as the rough and heterogeneous surface can cause insufficient coupling of the electrodes, which can result in poor data quality and noisy model interpretations. Nevertheless, an annually repeated pattern was detected at all sites, with increasing resistivity values in late

autumn and maximum values during winter (Fig. 8). The increase in resistivity is caused by a reduction of the liquid water content due to freezing processes. Even a small reduction in water content (< 1 %) due to freezing can cause an increase in resistivity of more than 50 % (e.g. Hilbich et al., 2011). At all sites, the highest resistivity values were found during the winter 2011/2012, which is caused by a thin and non-isolating snow cover (Fig. 8).

Below 3 m depth, seasonal changes in resistivity were only found for the Chastelets rock glacier (Fig. 7c), which are probably due to a seasonally changing amount of ice within the permafrost body.

5 Summary and conclusions

An extensive analysis of borehole temperature data of different periglacial materials by Schneider et al. (2012) recognized a need for more information about the subsurface material and composition to understand the spatially and temporally varying processes occurring in high-alpine permafrost regions. For that purpose borehole, ERT and RST measurements were performed from 2009 to 2012 within the same investigation area (Murtèl–Chastelets area in the eastern Swiss Alps). In addition a four-phase model was applied to calculate the volumetric fractions of ice, water and air. The surveys were focused on three different landforms (bedrock, talus slope and rock glacier) consisting of three different types of periglacial material (rock, coarse blocky boulders, fine-grained sediment). Based on the results of this study, the following conclusions can be drawn:

- Temperatures about -1°C below 3 m depth (Fig. 2c) and a resistive anomaly of approximately $30\text{ k}\Omega\text{m}$ (Fig. 3) confirm a permafrost occurrence of approximately 10–15 m thickness within the Chastelets rock glacier. It can be assumed that the permafrost body consists mainly of ice-cemented boulders, containing 35 % ice at maximum (Fig. 5).
- Within the fine-grained material (RCf), a layer with increased water content was recognized between 2 and 6 m depth. This might indicate a frozen layer below, which enables the water retention.
- The area of the Murtèl forefield consists predominantly of weathered bedrock with potentially water-filled cracks and partly covered with coarse boulders (Fig. 4). The talus slope was detected as a coarse blocky layer of only 2–3 m thickness, followed by bedrock underneath. The coarse blocky structure of this layer, in combination with the lateral effects through the internal air circulation within the talus slope, provokes a thermal regime which is able to sustain the permafrost beneath.
- During winter, the formation of seasonal ice within the active layer of the coarse blocky and fine-grained material was detected.
- Compared to the air temperature and the onset of the snow cover, the height of the winterly snow cover was detected as one of the most important factors, which influences the ground cooling.

The determination of geophysical properties of different periglacial materials is able to provide useful parameters for coupled hydro-thermal permafrost models and contributes to the general understanding of thermo-physical processes within the subsurface of high-mountain permafrost areas.

Especially the detection of small-scale features of high-alpine permafrost, such as the strongly weathered bedrock material at the bedrock site or the very shallow block cover near the talus slope borehole, remains challenging, but can be provided by geophysical surveys. However, uncertainties remain, as the strong surface heterogeneity impedes the coupling of the electrodes, which can cause poor data quality and noisy model interpretations of the subsurface. In addition, numerous factors can influence the inverted resistivity distribution (e.g. the measurement scheme or the regularization approach). To reduce these uncertainties, periodic measurements (bimonthly) were performed and mean values of extracted 2-D sections were used for data interpretation. Both approaches considerably improved the reliability of the results since a material-dependent annual range in specific resistivity could be determined and outliers could be identified.

Periodic RST measurements throughout the year would be valuable in addition to the ERT data in order to further verify the seasonal formation of ice.

Acknowledgements. The authors wish to express their thanks to all who assisted with the data acquisition in the field. Further we acknowledge the help of Michael Krautblatter and Daniel Draebing from the Department of Geography, University of Bonn, who conducted the laboratory analyses of seismic velocities of rock samples. This investigation was funded by the University of Fribourg, Switzerland, the German Research Foundation (DFG) through the SPCC project (Sensitivity of Mountain Permafrost to Climate Change, DFG HA3475/3-1) and the Swiss National Science Foundation through the Sinergia project TEMPS (The temporal evolution of mountain permafrost in Switzerland, CRSII2 136279). This article profited much from the comments of two anonymous reviewers.

Edited by: E. Reynard

Reviewed by: two anonymous referees

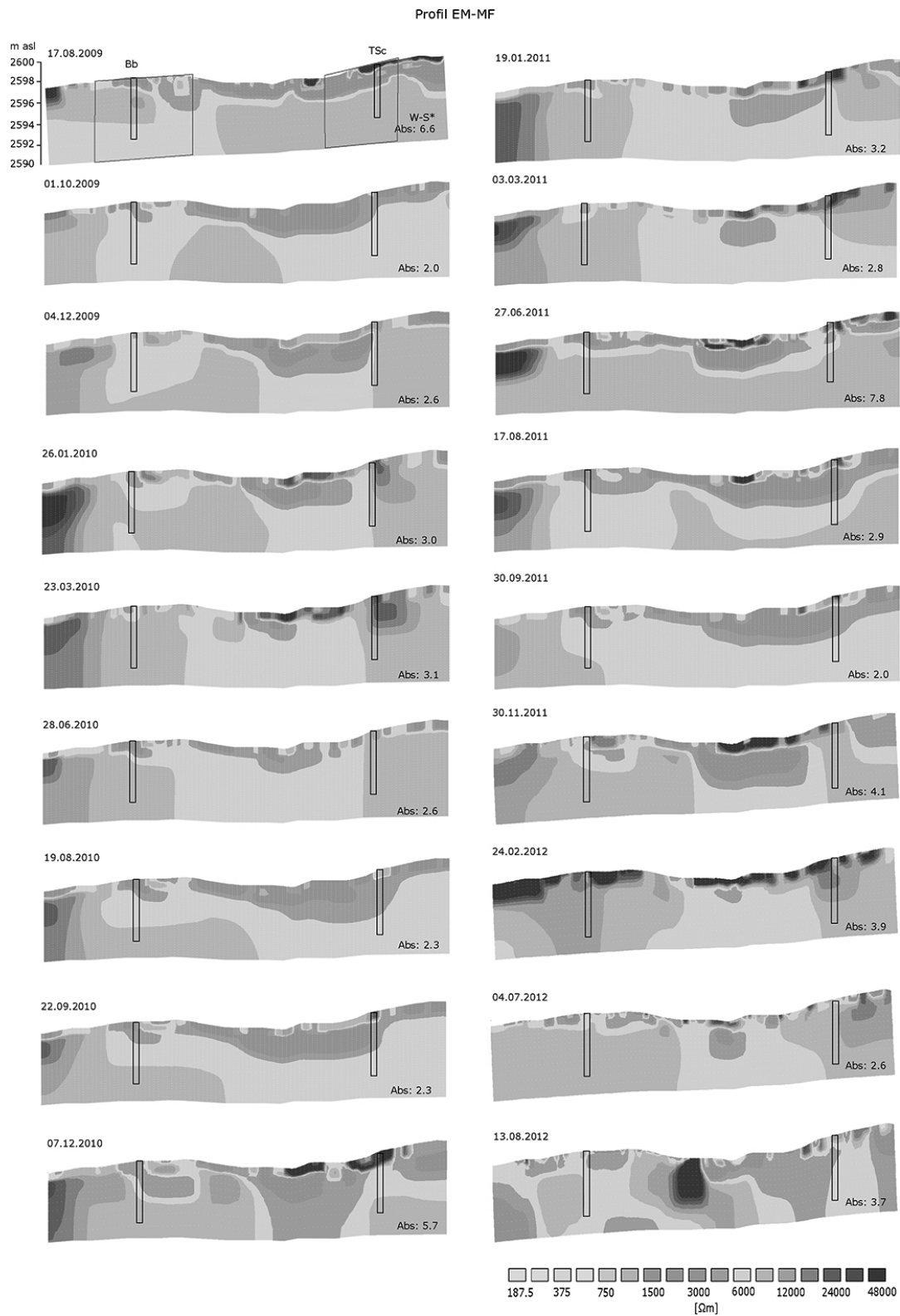


Figure A1. Inversion tomograms of the repeated ERTM measurements at the Murtèl forefield during the period of 2009 to 2012. The red rectangles mark the sections of the extracted measurement points. For every tomogram, the same sections were chosen. The error is given as absolute data misfit (Abs) in percent.

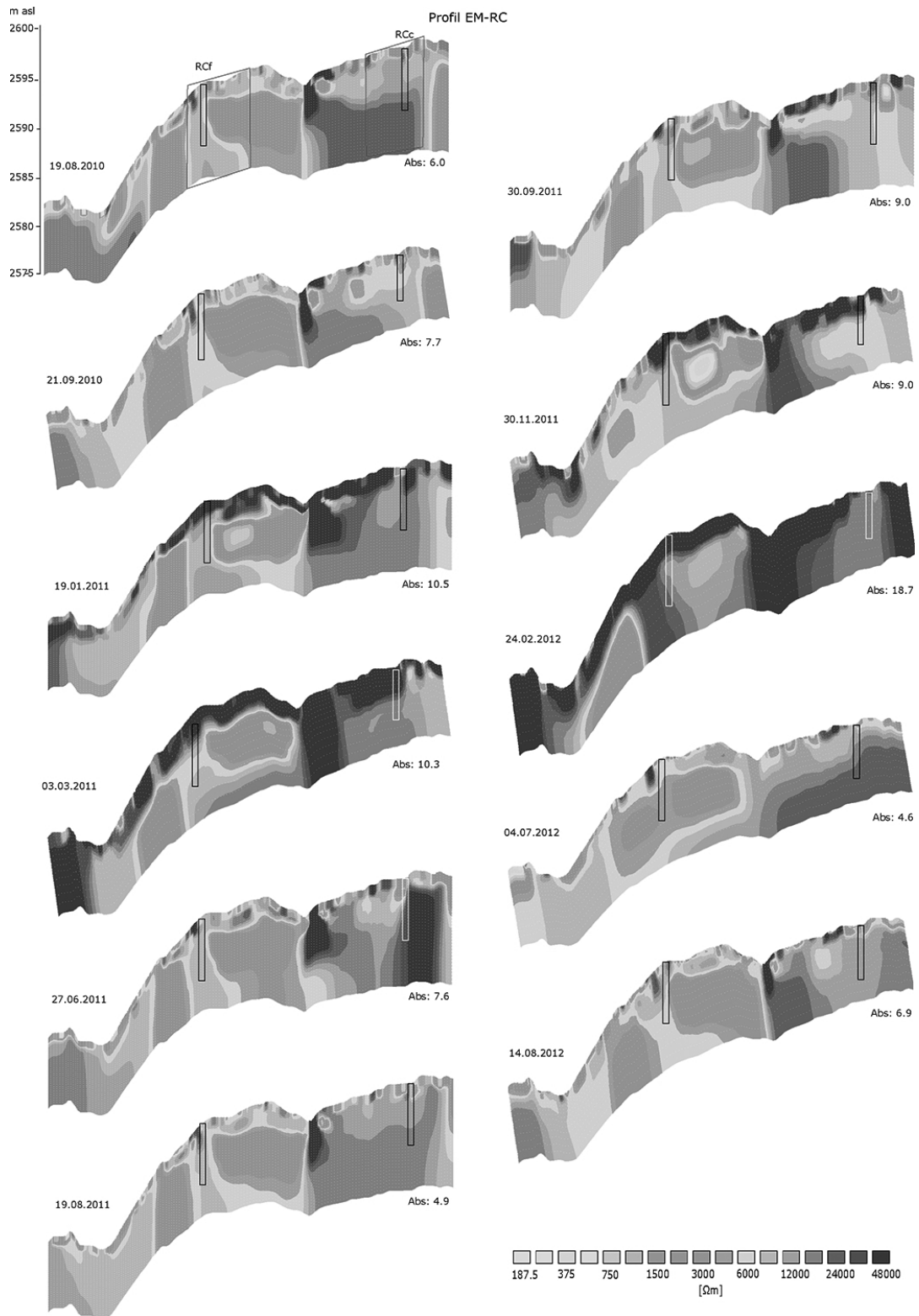


Figure B1. Inversion tomograms of the repeated ERTM measurements at the rock glacier Chastelets during the period of 2010 and 2012. The red rectangles mark the sections of the extracted measurement points. For every tomogram, the same sections were chosen. The error is given as absolute data misfit (Abs) in percent.

References

- Archie, G. E.: The electrical resistivity log as an aid in determining some reservoir characteristics, *Petroleum Transactions of American Institute of Mining and Metallurgical Engineers (AIME)*, 146, 54–62, 1942.
- Arenson, L. and Springman, S.: Triaxial constant stress and constant strain rate tests on ice-rich permafrost samples, *Can. Geotech. J.*, 42, 412–430, 2005.
- Barsch, D.: Refraktionsseismische Bestimmungen der Obergrenze des gefrorenen Schuttkörpers in verschiedenen Blockgletschern Graubündens, *Z. Gletscherkd. Glazialgeolog.*, 9, 143–167, 1973.
- deGroot Hedlin, G. and Constable, S. C.: Occam's inversion to generate smooth, two-dimensional models from magnetotelluric data, *Geophysics*, 55, 1613–1624, 1990.
- Delaloye, R. and Lambiel, C.: Evidence of winter ascending air circulation throughout talus slopes and rock glaciers situated in the lower belt of alpine discontinuous permafrost (Swiss Alps), *Norsk Geogr. Tidsskr.*, 59, 194–203, 2005.
- Fisch, W. and Haeberli, W.: Electrical DC resistivity soundings with long profiles on rock glaciers and moraines in the Alps of Switzerland, *Versuchsanst. für Wasserbau, Hydrologie u. Glaziologie an d. Eidg. Techn. Hochsch.*, 1977.
- Haerberli, W., Huder, J., Keusen, H., Pika, J., and Röthlisberger, H.: Core drilling through rock glacier-permafrost, in: 5th International Conference on Permafrost, Tapir Publishers, Trondheim, 937–942, 1988.
- Hanson, S. and Hoelzle, M.: Installation of a shallow borehole network and monitoring of the ground thermal regime of a high alpine discontinuous permafrost environment, *Norsk Geogr. Tidsskr.*, 59, 84–93, 2005.
- Hasler, A., Gruber, S., and Beutel, J.: Kinematics in permafrost bedrock, *J. Geophys. Res.*, 117, F01016, doi:10.1029/2011JF001981, 2012.
- Hauck, C.: Frozen ground monitoring using DC resistivity tomography, *Geophys. Res. Lett.*, 29(21), doi:10.1029/2002GL014995, 2002.
- Hauck, C. and Kneisel, C.: Quantifying the ice content in low-altitude scree slopes using geophysical methods, edited by: Hauck, C. and Kneisel, C., Cambridge University Press, 153–164, 2008a.
- Hauck, C. and Kneisel, C.: Applied geophysics in periglacial environments, Cambridge University Press, Cambridge, 2008b.
- Hauck, C. and Vonder Mühll, D.: Inversion and interpretation of two-dimensional geoelectrical measurements for detecting permafrost in mountainous regions, *Permafrost Periglac.*, 14, 305–318, 2003.
- Hauck, C., Vonder Mühll, D., and Maurer, H.: Using DC resistivity tomography to detect and characterize mountain permafrost, *Geophys. Prospect.*, 51, 273–284, 2003.
- Hauck, C., Isaksen, K., Vonder Mühll, D., and Sollid, L. J.: Geophysical surveys designed to delineate the altitudinal limit of mountain permafrost: an example from Jotunheimen, Norway, *Permafrost Periglac.*, 15, 191–205, 2004.
- Hauck, C., Böttcher, M., and Maurer, H.: A new model for estimating subsurface ice content based on combined electrical and seismic data sets, *The Cryosphere*, 5, 453–468, doi:10.5194/tc-5-453-2011, 2011.
- Hecht, S.: Fallbeispiele zur Anwendung refraktionsseismischer Methoden bei der Erkundung des oberflächennahen Untergrundes, *Z. Geomorphol., Supplement*, 123, 111–123, 2000.
- Hilbich, C.: Time-lapse refraction seismic tomography for the detection of ground ice degradation, *The Cryosphere*, 4, 243–259, doi:10.5194/tc-4-243-2010, 2010.
- Hilbich, C., Hauck, C., Delaloye, R., and Hoelzle, M.: A geoelectric monitoring network and resistivity-temperature relationships of different mountain permafrost sites in the Swiss Alps, in: *Proceedings of the 9th International Conference on Permafrost*, edited by: Kane, D. L. and Hinkel, K. M., Vol. 1, 699–704, Institute on Northern Engineering, University of Alaska, Fairbanks, 2008a.
- Hilbich, C., Hauck, C., Hoelzle, M., Scherler, M., Schudel, L., Völksch, I., Vonder Mühll, D., and Mäusbacher, R.: Monitoring mountain permafrost evolution using electrical resistivity tomography: A 7-year study of seasonal, annual, and long-term variations at Schilthorn, Swiss Alps, *J. Geophys. Res.*, 113, F01S90, doi:10.1029/2007JF000799, 2008b.
- Hilbich, C., Marescot, L., Hauck, C., Loke, M., and Mäusbacher, R.: Applicability of electrical resistivity tomography monitoring to coarse blocky and ice-rich permafrost landforms, *Permafrost Periglac.*, 20, 269–284, 2009.
- Hilbich, C., Fuss, C., and Hauck, C.: Automated time-lapse ERT for improved process analysis and monitoring of frozen ground, *Permafrost Periglac.*, 22, 306–319, 2011.
- Hoelzle, M. and Gruber, S.: Borehole and Ground Surface Temperatures and their relationship to meteorological conditions in the Swiss Alps, in: *Proceedings of the 9th International Conference on Permafrost*, edited by: Kane, D. L. and Hinkel, K. M., Vol. 1, 723–728, Institute on Northern Engineering, University of Alaska, Fairbanks, 2008.
- Hoelzle, M., Vonder Mühll, D., and Haerberli, W.: Thirty years of permafrost research in the Corvatsch-Furtschellas area, Eastern Swiss Alps: a review, *Norsk Geogr. Tidsskr.*, 56, 137–145, 2002.
- Jongmans, D., Ptilakis, K., Demanet, D., Raptakis, D., Riepl, J., Horrent, C., Tsokas, G., Lontzetidis, K., and Bard, P.-Y.: EUROSEISTEST: Determination of the geological structure of the volvi basin and validation of the basin response, *B. Seismol. Soc. Am.*, 88, 473–487, 1998.
- Kääb, A., Gudmundson, G. H., and Hoelzle, M.: Surface deformation of creeping mountain permafrost. Photogrammetric investigations on rock glacier Murtèl, Swiss Alps, in: *Proceedings of the 7th International Conference on Permafrost*, edited by: Lewkowitz, A. G. and Allard, M., Yellowknife, Canada, 531–537, 1998.
- King, L., Fisch, W., Haerberli, W., and Wächter, H.: Comparison of resistivity and radio-echo soundings on rock glacier permafrost, *Z. Gletscherkd. Glazialgeolog.*, 23, 77–97, 1987.
- King, M. S., Zimmerman, R. W., and Corwin, R. F.: Seismic and electrical properties of unconsolidated permafrost, *Geophys. Prospect.*, 36, 349–364, 1988.
- Kneisel, C.: Assessment of subsurface lithology in mountain environments using 2D resistivity imaging, *Geomorphology*, 80, 32–44, 2006.
- Kneisel, C., Hauck, C., Fortier, R., and Moorman, B.: Advances in geophysical methods for permafrost investigations, *Permafrost Periglac.*, 19, 157–178, 2008.
- Krautblatter, M.: Geophysical detection of rock mass instability, in: *Proceedings of the 9th International Conference on Permafrost*,

- edited by: Kane, D. L. and Hinkel, K. M., Vol. 1, 999–1004, Institute on Northern Engineering, University of Alaska, Fairbanks, 2008.
- Krautblatter, M., Verleysdonk, S., Flores-Orozco, A., and Kemna, A.: Temperature-calibrated imaging of seasonal changes in permafrost rock walls by quantitative electrical resistivity tomography (Zugspitze, German/Austrian Alps), *J.f Geophys. Res.*, 115, 306–319, doi:10.1029/2008JF001209, 2010.
- Lambiel, C. and Pieracci, K.: Permafrost distribution in talus slopes located within the alpine periglacial belt, Swiss Alps, *Permafrost Periglac.*, 19, 293–304, 2008.
- Loke, M. H.: Tutorial: 2-D and 3-D electrical imaging surveys, www.geoelectrical.com, 2011.
- Loke, M. H. and Barker, R. D.: Rapid least-squares inversion of apparent resistivity pseudosections using a quasi-Newton method, *Geophys. Prospect.*, 44, 131–152, 1996.
- Lugon, R., Delaloye, R., Serrano, E., Reynard, E., Lambiel, C., and González-Trueba, J.: Permafrost and Little Ice Age glacier relationships, Posets Massif, Central Pyrenees, Spain, *Permafrost Periglac.*, 15, 207–220, 2004.
- Marescot, L., Monnet, R., and Chapellier, D.: Resistivity and induced polarization surveys for slope instability studies in the Swiss Alps, *Eng. Geol.*, 98, 18–28, 2008.
- Matsuoka, N., Hirakawa, K., Watanabe, T., Haerberli, W., and Keller, F.: The role of diurnal, annual and millennial freeze-thaw cycles in controlling alpine slope stability, in: *Proceedings of the 7th International Conference on Permafrost*, edited by: Lewkowicz, A. G. and Allard, M., Yellowknife, Canada, 711–717, 1998.
- Maurer, H. and Hauck, C.: Geophysical imaging of alpine rock glaciers, *J. Glaciol.*, 53, 110–120, 2007.
- Morard, S.: Effets de la circulation d'air par effet de cheminée dans l'évolution du régime thermique des éboulis froids de basse et moyenne altitude, Ph.D. thesis, University of Fribourg, 2011.
- Musil, M., Maurer, H., Green, A. G., Horstmeyer, H., Nitsche, F., Vonder Mühll, D., and Springman, S.: Shallow seismic surveying of an Alpine rock glacier, *Geophysics*, 67, 1701–1710, 2002.
- Noetzi, J. and Vonder Mühll, D.: Permafrost in Switzerland 2006/2007 and 2007/2008, Glaciological Report (Permafrost), Vol. 8/9, Permafrost Monitoring Switzerland (PERMOS), Cryospheric Commission, University of Zürich, 2010.
- Otto, J. and Sass, O.: Comparing geophysical methods for talus slope investigations in the Turtmann valley (Swiss Alps), *Geomorphology*, 76, 257–272, 2006.
- Ottowitz, D., Jochum, B., Supper, R., Römer, A., Pfeiler, S., and Keuschnig, M.: Permafrost monitoring at Mölltaler Glacier and Magnetköpfl, *Berichte der Geologischen Bundesanstalt*, 93, 57–64, 2011.
- Pearson, C., Murphy, J., Halleck, P., Hermes, R., and Mathews, M.: Sonic and resistivity measurements on Berea sandstone containing tetrahydrofuran hydrates: a possible analog to natural gas hydrate deposits, in: *Proceedings of the 4th International Conference on Permafrost*, Fairbanks, Alaska, 973–978, 1983.
- Phillips, M., Ladner, F., Müller, M., Sambeth, U., Sorg, J., and Teysseire, P.: Monitoring and reconstruction of a chairlift midway station in creeping permafrost terrain, Grächen, Swiss Alps, *Cold Reg. Sci. Technol.*, 47, 32–42, 2007.
- Reynolds, J. M.: An introduction to applied and environmental geophysics, John Wiley and Sons Ltd, West Sussex, England, 2005.
- Ribolini, A., Guglielmin, M., Fabre, D., Bodin, X., Marchisio, M., Sartini, S., Spagnolo, M., and Schoeneich, P.: The internal structure of rock glaciers and recently deglaciated slopes as revealed by geoelectrical tomography: insights on permafrost and recent glacial evolution in the Central and Western Alps (Italy–France), *Quaternary Sci. Rev.*, 29, 507–521, 2010.
- Rode, M. and Sass, O.: Monitoring of water content, water displacement and freeze-thaw processes in alpine rock walls using geoelectric survey lines, in: *Geoelectric Monitoring – current research and perspectives for the future*, edited by: der Geologischen Bundesanstalt, B., Vol. 93, 204–211, 2011.
- Roedder, T.: Spatio-temporal assessment of dynamics in discontinuous mountain permafrost – Investigation of small-scale influences on the ground thermal regime and on active layer processes during snow melt, Ph.D. thesis, University of Würzburg, 2012.
- Roedder, T. and Kneisel, C.: Permafrost mapping using quasi-3D resistivity imaging, Murtèl, Swiss Alps, *Near Surf. Geophys.*, 10, 117–127, doi:10.3997/1873-0604.2011029, 2012.
- Sandmeier, K. J.: REFLEXW-Windows 9x/NT/2000/XP-program for the processing of seismic, acoustic or electromagnetic reflection, refraction and transmission data, software, <http://www.sandmeier-geo.de/>, 2010.
- Scapozza, C., Lambiel, C., Baron, L., Marescot, L., and Reynard, E.: Internal structure and permafrost distribution in two alpine periglacial talus slopes, Valais, Swiss Alps, *Geomorphology*, 132, 208–221, 2011.
- Schneider, S., Hoelzle, M., and Hauck, C.: Influence of surface and subsurface heterogeneity on observed borehole temperatures at a mountain permafrost site in the Upper Engadine, Swiss Alps, *The Cryosphere*, 6, 517–531, doi:10.5194/tc-6-517-2012, 2012.
- Scott, W., Sellmann, P., and Hunter, J.: Geophysics in the study of permafrost, *Geotechnical and Environmental Geophysics*, tulsa, 355–384, 1990.
- Timur, A.: Velocity of compressional waves in porous media at permafrost temperatures, *Geophysics*, 33, 584–595, 1968.
- Vonder Mühll, D. and Holub, P.: Borehole logging in alpine permafrost, Upper Engadin, Swiss Alps, *Permafrost Periglac.*, 3, 125–132, 1992.
- Vonder Mühll, D. and Klingele, E.: Gravimetrical investigation of ice rich permafrost within the rock glacier Murtèl-Corvatsch, *Permafrost Periglac.*, 5, 13–24, 1994.
- Vonder Mühll, D., Hauck, C., Gubler, H., McDonald, R., and Russell, N.: New geophysical methods of investigating the nature and distribution of mountain permafrost with special reference to radiometry techniques, *Permafrost Periglac.*, 12, 27–38, 2001.
- Wagner, S.: DC resistivity and seismic refraction soundings on rock glacier permafrost in northwestern Svalbard, *Norsk Geogr. Tidsskr.*, 50, 25–36, 1996.